Dirac multipoles in diffraction by the layered room-temperature antiferromagnets $BaMn_2P_2$ and $BaMn_2As_2$

S. W. Lovesey[1,2,*] and D. D. Khalyavin[1]
[1]*ISIS Facility, STFC, Oxfordshire OX11 0QX, England, United Kingdom*
[2]*Diamond Light Source, Ltd., Oxfordshire OX11 0DE, England, United Kingdom*

(Received 14 April 2018; revised manuscript received 25 July 2018; published 30 August 2018)

Properties of two $ThCr_2Si_2$-type materials are discussed within the context of their established structural and magnetic symmetries—the structure type accounts for more than 400 compounds of the AB_2X_2 composition. Both materials develop collinear, G-type antiferromagnetic order above room temperature, and magnetic ions occupy acentric sites in centrosymmetric structures (magnetic crystal class $4'/m'm'm$). We refute a previous conjecture that $BaMn_2As_2$ is an example of a magnetoelectric material with hexadecapole order using Dirac (magnetoelectric) multipoles by exposing flaws in supporting arguments: principally, an omission of discrete symmetries enforced by the symmetry ($\bar{4}m'2'$) of sites used by Mn ions and, also, improper classifications of the primary and secondary order parameters. G-type antiferromagnetism using conventional magnetic dipoles provides the primary order parameter. Dirac quadrupoles are secondary, and possibly visible in Bragg diffraction patterns. Patterns caused by conventional magnetic dipoles and Dirac multipoles are predicted to be fundamentally different, which raises the intriguing possibility of a unique and comprehensive examination of the magnetoelectric state by diffraction; Dirac multipoles create Bragg spots with Miller index l even (and $h + k$ even) while magnetic dipoles appear for l odd (and $h + k$ odd). A rotoinversion operation ($\bar{4}$) in Mn site symmetry is the ultimate source of distinguishing features in multipole types.

DOI: 10.1103/PhysRevB.98.054434

I. INTRODUCTION

Structural and magnetic properties of $BaMn_2P_2$ [1] and $BaMn_2As_2$ [2] are similar to those of the archetypal magnetoelectric material chromium sesquioxide, Cr_2O_3 [3,4]. For, the transition metal ions in these materials occupy acentric sites in centrosymmetric structures, and their magnetic dipole moments form simple antiferromagnetic patterns, with magnetic propagation vector $\mathbf{k} = (0, 0, 0)$, at relatively high temperatures. Moreover, the development of long-range magnetic order as a function of temperature is continuous, without a structural transition or distortion, and hysteresis is absent. While the pattern of dipole moments breaks both time-reversal symmetry and inversion symmetry that are present in the paramagnetic phase, the product of the two symmetries is not changed by the onset of magnetic order and the magnetoelectric property is allowed [5,6,7]. At an atomic level of detail, Cr ions in Cr_2O_3 are allowed parity-odd quadrupoles that can diffract x rays [8]. The same could be true of Mn ions in $BaMn_2P_2$ and $BaMn_2As_2$, according to calculations reported for $Ba_{1-x}Na_xFe_2As_2$ [9].

We offer a discussion of the magnetoelectric properties of $BaMn_2P_2$ and $BaMn_2As_2$ [1,2], which present small band-gap local moment semiconducting behavior, that is informed by magnetic symmetry in the footsteps of Dzyaloshinskii [4]. In this context, we recall the "totalitarian principle" attributed to Gell-Mann by which anything not forbidden (by symmetry) is compulsory [10], e.g., weak ferromagnetism and magnetic multipoles that are parity odd. (The multipoles in question are labeled magnetoelectric by some authors, although Dirac appears an equally sound label since the parity-odd (acentric) and time-odd (magnetic) monopole has discrete symmetries to match the Dirac monopole, which is yet to be observed [10].) The $ThCr_2Si_2$-type chemical structure ($I4/mmm$, #139) is illustrated in Fig. 1, together with the magnetic structure of interest ($I4'/m'm'm$, no. 139.536 [11]), while other physical properties of the materials are gathered in Table I. The $ThCr_2Si_2$-type structure is constructed from layers of edge sharing $BX_{4/4}$ tetrahedra alternating with Ba ions. At this point it is of interest to note some significant differences between $BaMn_2P_2$ and $BaMn_2As_2$ and isostructural $BaFe_2As_2$: specifically, $BaFe_2As_2$ presents metallic character and itinerant magnetism, a structural distortion, superconductivity, and moderate Fe-pnictogen hybridization, with approximately 10–20% As character in the d bands.

Referring to Fig. 1, manganese networks in $BaMn_2P_2$ and $BaMn_2As_2$ are square planar. Tetrahedral coordinated Mn ions, with acentric site symmetry $\bar{4}m2$, form Mn_2P_2 and Mn_2As_2 sheets separated by the cations. Ba cations sit in an eightfold cubic hole created by phosphorus or arsenide ions. The pattern of conventional magnetic dipoles, created from spin (**S**) and orbital (**L**) moments, aligned along the c axis is identical to well-known orthorhombic perovskites. It is G-type antiferromagnetism indexed on the chemical structure, with $I4'/m'm'm$ the appropriate magnetic space group. Saturation magnetic moments determined from neutron diffraction, listed in Table I, are smaller than the value for high-spin $Mn^{2+}(3d^5)$. The observed departure from a value $= 5\,\mu_B$ for the moment, derived using $S_z = 5/2$, can be attributed to covalency combined with antiferromagnetic order, and Hubbard and Marshall

*Corresponding author: stephen.lovesey@stfc.ac.uk

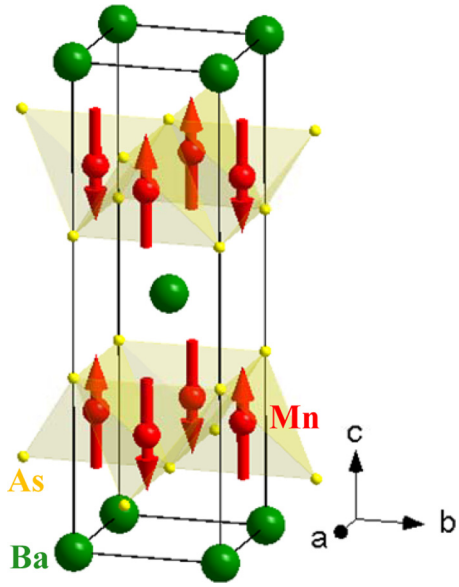

FIG. 1. Chemical ($I4/mmm$) and magnetic ($I4'/m'm'm$) structures of $BaMn_2As_2$ [2]. Red arrows denote Mn dipole moments parallel to the c axis in a G-type antiferromagnetic motif, with Ba ions (green) and As ions (yellow). Cartesian coordinates (x, y, z) used in the text coincide with cell edges.

discuss various consequences of covalent bonding depending on local crystal symmetry [12].

The objectives of our communication are, first, to correctly describe magnetic properties of the magnetoelectric materials $BaMn_2P_2$ and $BaMn_2As_2$ using existing experimental data [1,2], with attention to ubiquitous Dirac Mn multipoles and their possible exposure in future diffraction experiments; second, to describe a proper procedure for classifying magnetic order parameters in complex materials; and, third, to expose and correct fatal deficiencies in a published meta-analysis of magnetoelectric properties of $BaMn_2As_2$ [13].

TABLE I. $ThCr_2Si_2$-type magnetoelectric materials $BaMn_2P_2$ [1] and $BaMn_2As_2$ [2]. Data were gathered on powder samples using neutron Bragg diffraction. Space group $I4/mmm$ (no. 139, tetragonal $4/mmm$ crystal class, Miller indices $h+k+l$ even from I centering) with Mn in $4d$; Ba in $2a$; and P, As in $4e$. Magnetic space group $I4'/m'm'm$ (no. 139.536, $4'/m'm'm$ magnetoelectric crystal class) [11], with Mn dipole moments parallel to the c axis in a collinear G-type antiferromagnetic motif—magnetic propagation vector $\mathbf{k} = (0,0,0)$—and indexed by Miller indices $h+k$ odd and l odd. The saturation magnetic moment, μ, is less than $\approx 5\,\mu_B$ expected of the high-spin $Mn^{2+}(3d^5)$ configuration. A continuous magnetic phase transition, not exhibiting magnetic hysteresis, with no change in the structure or distortion of the lattice is inferred from experimental evidence. Approximate cell parameters a and c, and Néel temperature T_N.

Compound	a (Å)	c (Å)	$\mu(\mu_B)$	T_N(K)
$BaMn_2P_2$ [1]	4.04	13.05	4.2 (at $T \approx 293$ K)	>750
$BaMn_2As_2$ [2]	4.15	13.41	3.88 (at $T \approx 10$ K)	625

It is fitting to discuss magnetic properties of materials in terms of a unit-cell structure factor suitable for the interpretation of Bragg diffraction patterns, because well-established scattering techniques yield an abundance of information about magnetic materials. Watanabe and Yanase [13] have calculated Dirac multipoles that are directly relevant to a simulation of neutron diffraction, according to our calculations. The reported nonzero values are grounds for optimism about the success of experiments that we propose. Bulk properties, such as the magnetoelectric effect, are prescribed by the structure factor evaluated for zero deflection of the radiation, i.e., the forward direction. By definition, the unit-cell structure factor incorporates all elements of symmetry in a given magnetic structure, including discrete symmetries demanded by local environments at sites used by magnetic ions.

Watanabe and Yanase [13] identify the ground state of $BaMn_2As_2$ as a magnetic hexadecapole ordered state, in which the order parameter is derived from Dirac multipoles of fourth rank (unlike a conventional magnetic order parameter that is a motif of dipoles ($\mathbf{L} + 2\mathbf{S}$), which can be detected in the laboratory with a magnetometer). Their intriguing result, the first of its kind, is derived from a symmetry argument and extensive microscopic calculations. Our misgivings about the result are on two levels. In the first place, analogy with weak ferromagnetism in haematite (α-Fe_2O_3) [14], say, leads us to question their assertion that a weak magnetoelectric multipole is a relevant order parameter. The assertion would be justified if magnetic dipoles did not order. This extreme case is realized in the pseudogap phase of the ceramic superconductor Hg1201 where conventional, parity-even magnetism using Cu ions is forbidden by anti-inversion, $\bar{1}'$, in the Cu site symmetry, leaving Dirac multipoles as legitimate candidates for an order parameter [15]. No such finding for Hg1201 could be reached with the approach to magnetic properties adopted by Watanabe and Yanase [13], for their approach to magnetic properties omits magnetic site symmetry—Mn site symmetry in magnetic $BaMn_2As_2$—by which it is woefully deficient. The omission is a nontrivial shortcoming, because Mn site symmetry ($\bar{4}m'2'$) does not match the magnetic crystal class (point group) of the space group ($4'/m'm'm$). The deficiency and its consequences are made explicit in our calculations for $BaMn_2P_2$ and $BaMn_2As_2$ using a correct symmetry argument, i.e., all symmetry present in the appropriate magnetic space group. We conclude that the identification of a magnetic hexadecapole ordered state using Dirac multipoles is erroneous [13], with Dirac multipoles of lower rank present in both materials and potentially visible in diffraction experiments.

II. SYMMETRY INFORMED ANALYSIS

A standard example where primary and secondary magnetic order parameters are present is weak ferromagnetism allowed by symmetry in a magnetic space group, and possibly realized in a material by the action of a Dzyaloshinskii-Moriya asymmetric spin interaction. Such symmetry-allowed weak ferromagnetism is secondary to a primary magnetic-order manifest in a simple pattern of magnetic dipoles allowed by symmetry. The secondary order parameter is a coupling phenomenon and does not have its own instability even if the symmetries of the secondary and primary order parameters are identical. For

materials under discussion, G-type antiferromagnetism using conventional magnetic dipoles provides the primary order parameter, and Dirac multipoles are secondary.

Classifying Dirac multipoles as candidates for a primary order parameter would be justified if magnetic dipoles did not order. This extreme case is realized in the pseudogap phase of the ceramic superconductor Hg1201, where conventional parity-even magnetism using Cu ions is forbidden by anti-inversion, $\bar{1}'$, in the Cu site symmetry [15].

In the present case, Dirac multipoles are shown to contribute to diffraction patterns allowed by the chemical structure. Bragg spots indexed on the chemical structure and observed in the diffraction of neutrons arise from nuclear and magnetic amplitudes, the contributions of which can be resolved by polarization analysis. X-ray Bragg diffraction exploiting the intensity enhancement offered by an atomic resonance is possibly a better option for observation of Dirac multipoles.

An analysis of magnetic phenomena informed by symmetry is incomplete and, consequently, potentially misleading if it fails to impose all restrictions, or selection rules, demanded by elements of symmetry in the full magnetic space group, composed of rotations, inversions, time reversal, and translations. Failure to include discrete symmetries imposed by symmetry in the sites used by magnetic ions renders analysis of magnetic properties incomplete in all but one case. The singular case is that of identical site and space-group symmetries, which excludes Mn ions in $BaMn_2As_2$ and $BaMn_2P_2$. For the space group $I4/mmm$ used by these materials the singular case is realized by ions at Wyckoff sites $2a$ or $2b$ with symmetry $4/mmm$, whereas paramagnetic Mn ions actually use sites $4d$ that have a different symmetry, namely, $\bar{4}m2$. Our unit-cell structure factor for magnetic properties of $BaMn_2As_2$ and $BaMn_2P_2$, Eq. (2), complies with the full magnetic space group. It manifestly includes Mn site symmetry, because the expression in (2) is proportional to the Mn multipole that conforms to site symmetry $\bar{4}m'2'$.

III. DIFFRACTION AMPLITUDES

Electronic degrees of freedom of Mn ions are encapsulated in (irreducible) spherical multipoles $\langle \mathrm{O^K_Q} \rangle$, where $\langle \ldots \rangle$ denotes an expectation value (time average) and the integer K is the multipole rank, with projections $-K \leqslant Q \leqslant K$. In the electronic structure factor,

$$\Psi^{\mathrm{K}}{}_{\mathrm{Q}} = \sum_{\mathbf{d}} \exp(\mathrm{i}\mathbf{d} \bullet \tau) \left\langle \mathrm{O}^{K}{}_{\mathrm{Q}} \right\rangle_{\mathbf{d}}, \tag{1}$$

the sum is over sites labeled **d** in the magnetic unit cell used by Mn ions, namely, Wyckoff $4d$ in $I4'/m'm'm$. The Bragg wave vector $\tau = (h, k, l)$, and I centering demands the condition $h + k + l$ even on the integer Miller indices. One finds

$$\Psi^{\mathrm{K}}{}_{\mathrm{Q}} = 2 \left\langle \mathrm{O^K_Q} \right\rangle \exp(\mathrm{i}\pi l/2)(-1)^k [1 + (-1)^l \sigma_\theta \sigma_\pi], \tag{2}$$

where σ_θ (time) and σ_π (parity) are signatures $= \pm 1$ of the discrete symmetries of $\langle \mathrm{O^K_Q} \rangle$. In subsequent working, we employ specific symbols for multipoles with different discrete symmetries and different definitions. Specifically, $\langle \mathrm{T^K_Q} \rangle$ and $\langle \mathrm{H^K_Q} \rangle$ are parity even and parity odd, respectively, in magnetic neutron scattering, and $\langle \mathrm{G^K_Q} \rangle$ is both parity odd and time odd in resonance-enhanced x-ray diffraction. The definitions of $\langle \mathrm{H^K_Q} \rangle$ and $\langle \mathrm{G^K_Q} \rangle$ mean that they are specific examples of Dirac multipoles.

Evaluated for the paramagnetic region, with $\sigma_\theta = +1$, $\Psi^{\mathrm{K}}{}_{\mathrm{Q}}$ is identical to the result published previously [9]. The four sites in the unit cell that contribute in (2) are

$$(1/2, 0, 1/4) \uparrow, (1/2, 0, 3/4) \downarrow, (0, 1/2, 3/4) \times \uparrow, (0, 1/2, 1/4) \downarrow,$$

and arrows indicate relative moment directions along the c axis. Environments at the first pair of sites are related by the operation $2_{\mathrm{y}} \equiv m'_z$, where Cartesian coordinates (x, y, z) coincide with cell edges in Fig. 1, and the second pair is displaced by $(1/2, 1/2, 1/2)$. The results,

$$\left\langle \mathrm{O^K}{}_{-\mathrm{Q}} \right\rangle = (-1)^{\mathrm{K}} \sigma_\theta \sigma_\pi \left\langle \mathrm{O^K_Q} \right\rangle, (-1)^{\mathrm{p}} = \sigma_\pi, \text{with} Q = \pm 2\mathrm{p}, \tag{3}$$

are required by site symmetry $\bar{4}\mathrm{m}'2'$ [11], and they are used in the derivation of (2). Setting Miller indices equal to zero in (2) shows that the unit-cell structure factor for bulk properties vanishes for conventional magnetic multipoles ($\sigma_\theta = -1$, $\sigma_\pi = +1$), as expected for compensated magnetic order. It is different from zero for Dirac multipoles that are both time odd ($\sigma_\theta = -1$) and parity odd ($\sigma_\pi = -1$), because the magnetic crystal class $4'/m'm'm$ is one of the 58 crystal classes that allow the linear magnetoelectric effect. Dirac monopoles and dipoles (also called anapoles or toroidal dipoles) are forbidden, because $|\mathrm{Q}| = 2$ is a minimum magnitude of projections when $\sigma_\pi = -1$. The electronic structure factor (2) is proportional to the Mn multipole. This result is explicit proof that discrete symmetries required by $\bar{4}m'2'$ are necessary to get the complete description of the magnetic properties of $BaMn_2P_2$ and $BaMn_2As_2$, including their bulk properties.

Amplitudes for x-ray or neutron diffraction derived from (2) contain Hermitian multipoles only, for which $\langle \mathrm{O^K}{}_{-\mathrm{Q}} \rangle = (-1)^{\mathrm{Q}} \langle \mathrm{O^K_Q} \rangle^*$ and identities,

$$\left\langle \mathrm{O^K}{}_{-\mathrm{Q}} \right\rangle = \left\langle \mathrm{O^K_Q} \right\rangle^* = (-1)^{\mathrm{K}} \sigma_\theta \sigma_\pi \left\langle \mathrm{O^K_Q} \right\rangle, \tag{4}$$

follow through correct use of (3). Parity-even multipoles, with $\sigma_\theta = -1$ & $\sigma_\pi = +1$, that deflect neutrons, $\langle \mathrm{T^K}{}_Q \rangle$, are purely real (imaginary) for K odd (even), and the allowed projections include $\mathrm{Q} = 0, \pm 4$. A dipole $\langle T^1{}_0 \rangle \equiv \langle T^1{}_z \rangle$ is proportional to the magnetic moment, in a first approximation.

IV. NEUTRON DIFFRACTION

Neutron polarization analysis can be used to extract the magnetic contribution to the intensity of a Bragg spot with overlapping nuclear and magnetic amplitudes. Primary and secondary polarizations are **P** and **P′**, and a fraction $(1 - \mathbf{P} \bullet \mathbf{P}')/2$ of neutrons participate in events that change (flip) the neutron spin orientation. For a collinear magnetic motif one finds $(1 - \mathbf{P} \bullet \mathbf{P}')/2 \propto \{(1/2)(1 + \mathrm{P}^2) |\langle \mathbf{Q}_\perp \rangle|^2 - |\mathbf{P} \bullet \langle \mathbf{Q}_\perp \rangle|^2\}$. A quantity $\mathrm{SF} = |\langle \mathbf{Q}_\perp \rangle - \mathbf{P}(\mathbf{P} \bullet \langle \mathbf{Q}_\perp \rangle)|^2$ obtained with $\mathrm{P}^2 = 1$ is a convenient measure of the strength of spin-flip scattering.

Bragg spots created by conventional magnetic multipoles are indexed by $h + k$ odd and l odd, whereas Bragg spots created by Dirac multipoles are indexed by $h + k$ even and l even. The magnetic neutron scattering amplitude

$\langle \mathbf{Q}_\perp \rangle = [\boldsymbol{\kappa} \times (\langle \mathbf{Q} \rangle \times \boldsymbol{\kappa})]$ where $\boldsymbol{\kappa}$ is a unit vector in the direction of the Bragg wave vector, $\boldsymbol{\kappa} = \boldsymbol{\tau}(h,k,l)/|\boldsymbol{\tau}(h,k,l)|$. For the parity-even intermediate amplitude (l odd),

$$\langle \mathbf{Q} \rangle^{(+)} = 4\exp(\mathrm{i}\pi l/2)(-1)^k \langle j_0(k) \rangle (g/2)(0,0,\langle S_z \rangle), \quad (5)$$

and the equation applies to ^6S for Mn^{2+} ($3d^5$) with no orbital angular momentum $\langle \mathbf{L} \rangle = 0$ and a gyromagnetic factor $g = 2.0$. In this expression, k is the magnitude of $\tau(h,k,l)$, and $\langle j_0(k) \rangle$ is a standard radial integral defined such that $\langle j_0(0) \rangle = 1$ [16]. However, $\langle \mathbf{Q} \rangle^{(+)}$ contains additional multipoles for all atomic configurations other than a pure s state, and they are accompanied by radial integrals $\langle j_n(k) \rangle$ with $n = 2, 4, \ldots$ that vanish at $k = 0$ [17,18]. More generally, the so-called dipole approximation,

$$\langle \mathbf{T}^1 \rangle \approx (3/2)[2\langle \mathrm{S} \rangle \langle \mathrm{j_0(k)} \rangle + \langle \mathbf{L} \rangle \{ \langle \mathrm{j_0(k)} \rangle + \langle \mathrm{j_2(k)} \rangle \}], \quad (6)$$

with $\langle j_2(0) \rangle = 0$ is useful, and

$$\langle \mathbf{Q} \rangle^{(+)} \approx (C/3)\left(0,0,\langle \mathrm{T}^1{}_z \rangle\right) \text{ with } \mathrm{C} = 4\exp(\mathrm{i}\pi l/2)(-1)^k. \quad (7)$$

The factor C is purely imaginary in the present case, $h+k$ odd and l odd. Electronic states with like parities make contributions to $\langle \mathbf{Q} \rangle^{(+)}$. Multipoles with an even rank, quadrupoles ($K = 2$), and hexadecapoles ($K = 4$) measure J mixing in allowed states since even rank $\langle \mathbf{T}^{\mathrm{K}} \rangle$ are zero within a J manifold [17,18].

Confining our immediate attention to multipoles up to and including octupoles allowed in the magnetic space group $I4'/m'm'm$, parity-even magnetic amplitudes are (l odd)

$$\begin{aligned}
\langle \mathbf{Q}_\mathrm{x} \rangle^{(+)} &\approx -\mathrm{C}(3/4)\sqrt{7}\kappa_\mathrm{x}\kappa_\mathrm{z}\langle \mathrm{T}^3{}_0 \rangle, \\
\langle \mathbf{Q}_\mathrm{y} \rangle^{(+)} &\approx -\mathrm{C}(3/4)\sqrt{7}\kappa_\mathrm{y}\kappa_\mathrm{z}\langle \mathrm{T}^3{}_0 \rangle, \\
\langle \mathbf{Q}_\mathrm{z} \rangle^{(+)} &\approx \mathrm{C}(3/2)\left[\langle \mathrm{T}^1{}_\mathrm{z} \rangle + (1/4)\sqrt{7}\left(3{\kappa_\mathrm{z}}^2 - 1\right)\langle \mathrm{T}^3{}_0 \rangle\right]. \quad (8)
\end{aligned}$$

The octupole, $\langle T^3{}_0 \rangle$, is purely real and a linear combination of radial integrals $\langle j_2(k) \rangle$ and $\langle j_4(k) \rangle$. It is identically zero for a pure s-state ion. In the event that $\langle T^3{}_0 \rangle$ is different from zero, because the manganese ion configuration departs from a pure s state, one or other of the contributions $\langle \mathbf{Q}_\mathrm{x}{}^{(+)} \rangle$ and $\langle \mathbf{Q}_\mathrm{y}{}^{(+)} \rangle$ will contribute at allowed Bragg spots since they are indexed by $\kappa_\mathrm{z} \propto l$ odd, and $h+k$ odd. The allowed hexadecapole, $\langle \mathrm{T}^4{}_{+4} \rangle$, not included in (8), is purely imaginary and has its origin in the orbital-spin part of the neutron electron interaction about which we have more to say in the context of Dirac multipoles.

Neutron diffraction by Dirac multipoles at sites occupied by Mn ions in $BaMn_2P_2$ and $BaMn_2As_2$ is determined by the amplitudes,

$$\begin{aligned}
\langle \mathbf{Q}_\mathrm{x} \rangle^{(-)} &= \mathrm{C}\ \kappa_\mathrm{x}\left[\mathrm{Z}_0 - \mathrm{Z}_1\left(5{\kappa_\mathrm{z}}^2 - 1\right) + \mathrm{Z}_3\left({\kappa_\mathrm{x}}^2 - 3{\kappa_\mathrm{y}}^2\right)\right], \\
\langle \mathbf{Q}_\mathrm{y} \rangle^{(-)} &= \mathrm{C}\ \kappa_\mathrm{y}\left[-\mathrm{Z}_0 + \mathrm{Z}_1\left(5{\kappa_\mathrm{z}}^2 - 1\right) + \mathrm{Z}_3\left(3{\kappa_\mathrm{x}}^2 - {\kappa_\mathrm{y}}^2\right)\right], \\
\langle \mathbf{Q}_\mathrm{z} \rangle^{(-)} &= \mathrm{C}\,\mathrm{Z}_2\kappa_\mathrm{z}\left({\kappa_\mathrm{x}}^2 - {\kappa_\mathrm{y}}^2\right), \quad (9)
\end{aligned}$$

that contain all the allowed multipoles. The factor C is purely real for l even ($h+k$ even). The quantity Z_0 contains only quadrupoles (K = 2), while Z_1, Z_2, and Z_3 are linear combinations of quadrupoles, octupoles (K = 3), and hexadecapoles (K = 4). Bragg spots (0, 0, l) have no magnetic intensity, while $\langle \mathbf{Q}_\mathrm{x} \rangle^{(-)} = -\langle \mathbf{Q}_\mathrm{y} \rangle^{(-)}$ with $\langle \mathbf{Q}_\mathrm{z} \rangle^{(-)} = 0$ for $(h,h,0)$ leads to $|\langle \mathbf{Q}_\perp \rangle^{(-)}|^2 = \mathrm{C}^2[\mathrm{Z}_0 + \mathrm{Z}_1 - \mathrm{Z}_3]^2$. Regarding spin-flip scattering, $\mathrm{SF}(h,h,0) = |\langle \mathbf{Q}_\perp \rangle^{(-)}|^2$ for (a) neutron polarization $\mathbf{P}$ parallel to $\boldsymbol{\kappa}$ and (b) $\mathbf{P}$ normal to the plane of scattering ($\mathbf{P} \bullet \boldsymbol{\kappa} = 0$), whereas $\mathrm{SF}(h,h,0) = 0$ for (c) $\mathbf{P}$ in the plane of scattering so that $\mathbf{P} \bullet \kappa = 0$. Results quoted for the three values of the polarization, labeled (a), (b), and (c), illustrate a general condition $\mathrm{SF_a} = \mathrm{SF_b} + \mathrm{SF_c}$.

Complete details of Dirac multipoles in neutron scattering, and the accompanying radial integrals, are found in Refs. [18,19]. By way of relevant examples,

$$\begin{aligned}
\left\langle \mathrm{H}^2{}_{+2}(3) \right\rangle' &= (1/2)\,(\mathrm{h_3})\sqrt{(5/6)}\big\langle -2(\mathrm{S_x n_x} - \mathrm{S_y n_y}) \\
&\quad + 5\left(\mathrm{n_x}^2 - \mathrm{n_y}^2\right)(\mathbf{S} \bullet \mathbf{n})\big\rangle, \\
\left\langle \mathrm{H}^3{}_{+2}(3) \right\rangle'' &= (7/2)\,(\mathrm{h_3})\sqrt{(5/6)}\big\langle \mathrm{S_x n_x}\left(1 - 3\mathrm{n_y}^2\right) \\
&\quad - \mathrm{S_y n_y}\left(1 - 3\mathrm{n_x}^2\right) - \left(\mathrm{n_x}^2 - \mathrm{n_y}^2\right)(\mathbf{S} \bullet \mathbf{n})\big\rangle, \\
\left\langle \mathrm{H}^4{}_{+2}(3) \right\rangle' &= (1/2)\,(\mathrm{h_3})\sqrt{(15/2)}\big\langle \mathrm{S_x n_x}\left(3 - 7\mathrm{n_x}^2\right) \\
&\quad - \mathrm{S_y n_y}\left(3 - 7\mathrm{n_y}^2\right) + 3\left(\mathrm{n_x}^2 - \mathrm{n_y}^2\right)(\mathbf{S} \bullet \mathbf{n})\big\rangle \quad (10)
\end{aligned}$$

occur in Z_1, Z_2, and Z_3. In these expressions for multipoles $\langle \mathrm{H}^{\mathrm{K}'}{}_{+2}(\mathrm{K}) \rangle$, $\mathbf{n}$ is a unit vector for the position of an electron, and $'$ ($''$) denotes the real (imaginary) part of a multipole. Irreducible multipoles created from a tensor product are discussed in the Appendix, with $\mathbf{H}^{\mathrm{K}'}(\mathrm{K})$ tensor products of $\mathbf{S}$ and a normalized spherical harmonic $\mathbf{C}^{\mathrm{K}}(\mathbf{n})$. In consequence, $\mathrm{K}' = \mathrm{K} - 1,\ \mathrm{K},\ \mathrm{K} + 1$ with K odd in a parity-odd multipole. Careful calculations of Dirac multipoles for different materials are reported in several works, including Refs. [13,20,21,22].

The contribution $\langle ({n_x}^2 - {n_y}^2)\mathrm{S_z n_z} \rangle$ to Dirac multipoles in (10) might be particularly large, because S_z could be assigned a value close to 5/2 in a naive estimation, and it occurs in the quadrupole, octupole, and hexadecapole. The expectation value in question occurs in the ratios 5: 7: − 9 in $\langle H^2{}_{+2}(3) \rangle' : \langle H^3{}_{+2}(3) \rangle'' : \langle H^4{}_{+2}(3) \rangle'$.

Previously, the contribution $\langle (\mathrm{n_x}^2 - \mathrm{n_y}^2)\mathrm{S_z n_z} \rangle$ was erroneously identified as a unique hexadecapole (K = 4) order parameter, whereas it is shown by us to contribute to irreducible multipoles of order K = 2 and 3 in addition [13]. Note that $\langle H^4{}_{+2}(3) \rangle' = (1/2)(\mathrm{h_3})\sqrt{(3/2)}\langle M^+{}_{42} \rangle$, where $\mathrm{M}^+{}_{42}$ appears in the list of unique magnetic multipoles provided in Table II in Ref. [13].

Radial integrals $(\mathrm{j_n})$ and $(\mathrm{h_n})$ in (10) and (11) are formed with radial densities that belong to states with opposite parities, and some illustrative examples are found in Ref. [18]. Substantial spin-dependent hybridization between d and pnictogen p states is reported from simulations of the electronic structure of $BaMn_2As_2$—stronger hybridization than in the antimonide [23]. Similar behavior is reported for the phosphor compound [24]. One finds $(\mathrm{j_2}) \rightarrow (\mathrm{k}\langle 3\mathrm{d}|\mathrm{R}|4\mathrm{p} \rangle)/15$ for small values of $\mathrm{ka_o}$, where $\mathrm{a_o}$ is the Bohr radius. Contributions to the electric dipole moment $\langle 3\mathrm{d}|\mathrm{R}|4\mathrm{p} \rangle$ are discussed in Ref. [19]. To the extent that radial wave functions are sensibly hydrogenic in form, $\langle 3\mathrm{d}|\mathrm{R}|4\mathrm{p} \rangle$ is proportional to $1/\mathrm{Z_c}$ where $\mathrm{Z_c}$ is the effective core charge seen by the electron. Explicit calculations using hydrogenic radial densities yield the results $(\mathrm{h_1}) \rightarrow 0.43(\mathrm{ka_o/Z_c})$, $(\mathrm{j_2}) \rightarrow (1/5)(\mathrm{h_1})$ and $(\mathrm{h_3}) \rightarrow 16.03(\mathrm{ka_o/Z_c})^3$ for small $\mathrm{ka_o}$.

V. X-RAY DIFFRACTION

Studies of various materials using resonant x-ray Bragg diffraction, accompanied by supporting calculations, are reported in Refs. [8,17,25–29], among many others. The scattering amplitude derived from quantum electrodynamics is developed in the small quantity E/mc^2 where E is the primary energy and $mc^2 = 0.511\,\mathrm{MeV}$ [17]. At the second level of smallness in this quantity the amplitude contains resonant processes that may dominate all other contributions should E match an atomic resonance Δ. Assuming also that virtual intermediate states are spherically symmetric, the scattering amplitude $\approx\{\mathrm{F}_{\mu'\nu}/(E-\Delta+i\Gamma/2)\}$ in the region of the resonance, where Γ is the total width of the resonance. Intensity of a Bragg spot is proportional to $|\mathrm{F}_{\mu'\nu}/(E-\Delta+\mathrm{i}\Gamma/2)|^2$. The numerator $\mathrm{F}_{\mu'\nu}$ is a unit-cell structure factor for Bragg diffraction in the scattering channel with primary (secondary) polarization ν (μ'). In keeping with convention, σ denotes polarization normal to the plane of scattering, and π denotes polarization within the plane of scattering. Our unit-cell structure factors include their dependence on a rotation of the crystal through an angle ψ around the Bragg wave vector in a so-called azimuthal-angle scan. The Bragg angle is denoted by θ and the primary beam is deflected through an angle 2θ.

An electric dipole–electric quadrupole (E1-E2) event gives access to Dirac multipoles that have ranks $K = 1, 2$, and 3, and they have been labeled $\langle G^{\mathrm{K}}{}_{\mathrm{Q}}\rangle$ [17]. Since magnetic symmetry restricts projections Q to ± 2, the anapole is forbidden. Bragg diffraction enhanced by the Mn L edges at $\Delta \approx 0.65\,\mathrm{keV}$ is not possible, since reflections are not within the Ewald sphere. In consequence, we consider enhancement at the Mn K edge at $\Delta \approx 6.54\,\mathrm{keV}$, which equates to a photon wavelength $\approx$1.90 Å. In so far as hydrogenic forms of radial wave functions are appropriate for the photoejected electron and empty valence states, radial matrix elements in an E1-E2 event are $\langle 1\mathrm{s}|\mathrm{R}|4\mathrm{p}\rangle = 0.30(\mathrm{a_o}/\mathrm{Z_c})$ and $\langle 1\mathrm{s}|\mathrm{R}^2|3\mathrm{d}\rangle = 1.73(\mathrm{a_o}/\mathrm{Z_c})^2$. Interference between parity-even (E2-E2) and parity-odd (E1-E2) diffraction amplitudes reported for corundumlike materials (V_2O_3 and α-Fe_2O_3) will not occur in diffraction by the materials of interest here, because our two amplitudes are indexed by different Miller indices, namely, l odd (E2-E2) and l even (E1-E2) [8].

K-edge amplitudes for Bragg diffraction are composed of $\langle \mathbf{G}^2\rangle \propto \langle\{\mathbf{L}\otimes\mathbf{n}\}^2\rangle$ and $\langle \mathbf{G}^3\rangle \propto \langle\{\{\mathbf{L}\otimes\mathbf{L}\}^2\otimes\mathbf{\Omega}\}^3\rangle$, where the orbital anapole $\mathbf{\Omega} = \mathrm{i}[\mathbf{L}^2,\mathbf{n}] = (\mathbf{L}\,\mathbf{x}\,\mathbf{n} - \mathbf{n}\,\mathbf{x}\,\mathbf{L})$. By way of illustrating the information content of E1-E2 unit-cell structure factors, let us consider Bragg spots indexed by Miller indices $l = 0$ and $h = k$. Structure factors are found to be

$$\begin{aligned}\mathrm{F}_{\sigma'\sigma}(h,h,0) &= (\mathrm{C}/\sqrt{15})\cos(\theta)\sin(\psi)\\ &\quad\times\left[\sqrt{2}\langle \mathrm{G}^2{}_{+2}\rangle' + (3\cos(2\psi)+1)\langle \mathrm{G}^3{}_{+2}\rangle''\right],\\ \mathrm{F}_{\pi'\sigma}(h,h,0) &= (\mathrm{C}/2\sqrt{15})\sin(2\theta)\cos(\psi)\left[2\sqrt{2}\langle \mathrm{G}^2{}_{+2}\rangle'\right.\\ &\quad\left.+\,(3\cos(2\psi)-1)\langle \mathrm{G}^3{}_{+2}\rangle''\right]. \qquad (11)\end{aligned}$$

Enhancement at the Mn K edge gives access to reflections with $h = 1$, 2, and 3. Azimuthal-angle scans in the unrotated and rotated channels of polarization evidently provide excellent opportunities to determine a relative strength for the Dirac quadrupole and octupole. The rotated channel does not contain Thompson scattering, which is an advantage when contributions from weak Dirac multipoles are of interest. To illustrate the pronounced sensitivity to the ratio of the two multipoles of intensity in a Bragg spot observed within the rotated channel of polarization, Fig. 2 displays a reduced version of $|F_{\pi'\sigma}(h,h,0)|^2$ as a function of the azimuthal angle for $\mathrm{p} = (\langle G^3{}_{+2}\rangle''/(\langle G^2{}_{+2}\rangle' 2\sqrt{2})) = 0.5$ and -0.5. By contrast, Bragg spots indexed by (0, 0, l) are much less useful, because the two multipoles in $\mathrm{F}_{\pi'\sigma}$ possess identical azimuthal-angle dependences. One finds

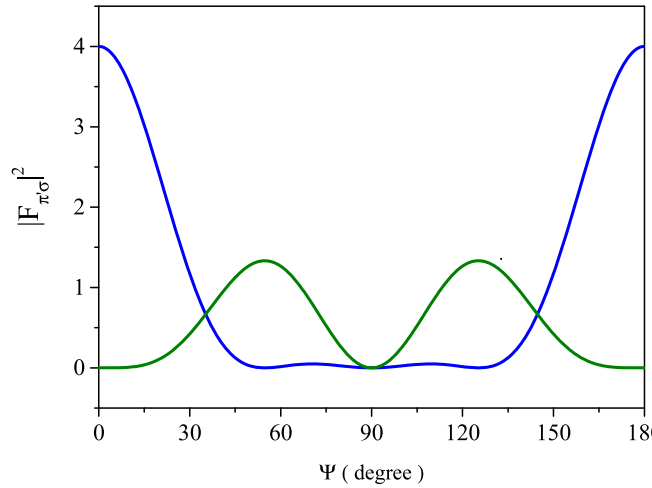

FIG. 2. Bragg spots $(h, h, 0)$ at which diffraction by conventional (parity-even) magnetism is forbidden. Intensity in the rotated channel of polarization $|F_{\pi'\sigma}|^2$ is illustrated as a function of the azimuthal angle ψ, using an expression derived from (11). The c axis is normal to the plane of scattering and parallel to σ polarization. The quantity $p = (\langle G^3{}_{+2}\rangle''/(\langle G^2{}_{+2}\rangle' 2\sqrt{2}))$ takes two values: $p = 0.50$ (blue line) and $p = -0.50$ (green line). The actual function displayed in the figure is $(\cos(\psi)\{1 + [3\cos(2\psi) - 1]p\})^2$ with ψ in the range $0 - 180^\circ$.

$$\begin{aligned}\mathrm{F}_{\pi'\sigma}(0,0,l) &= (C/\sqrt{30})\cos^2(\theta)\cos(2\psi)\left[\langle \mathrm{G}^2{}_{+2}\rangle'\right.\\ &\quad\left.-\,4\sqrt{2}\langle \mathrm{G}^3{}_{+2}\rangle''\right], \qquad (12)\end{aligned}$$

with l an even integer. At the origin of the azimuthal-angle scan, $\psi = 0$, the crystal a axis is normal to the plane of scattering. The twofold symmetry of $\mathrm{F}_{\pi'\sigma}(0,0,l)$ with respect to ψ is expected from the symmetry of a Mn environment. Results (11) and (12) apply to both materials of interest.

VI. DISCUSSION

Magnetoelectric properties of the layered, room-temperature antiferromagnets $BaMn_2P_2$ and $BaMn_2As_2$ are discussed making full use of information in the relevant magnetic space group. The space group $I4'/m'm'm$ (no. 139.536 [11]), with Mn ions using Wyckoff positions $4d$, is derived from knowledge of the chemical and magnetic structures reported in accounts of previous diffraction experiments [1,2]. We go on to predict effects in neutron and resonant x-ray Bragg diffraction patterns that are unique signatures of a magnetoelectric state that supports Mn Dirac multipoles, which are time odd (magnetic) and parity odd

(acentric). It is shown that the pattern of Bragg spots caused by Dirac multipoles and the pattern caused by a G-type antiferromagnetic order of conventional magnetic dipoles (time odd and parity even) are distinguishable, with Miller index l even in one case and odd in the other. An improper rotation in Mn site symmetry, the unique rotoinversion $\bar{4}$, lies at the heart of the distinction in diffraction patterns.

For x-ray resonant Bragg diffraction we predict great sensitivity in azimuthal-angle scans, where the crystal is rotated about the Bragg wave vector, to the relative size of Dirac multipoles. Structure factors for neutron diffraction that we report are exact, and contain all Dirac multipoles allowed by symmetry. In turn, we are in a position to give a complete study of spin-flip scattering obtained from neutron polarization analysis [30].

The existence of Dirac multipoles in a simulation of the electronic structure of $BaMn_2As_2$ [13] supports the feasibility of the diffraction experiments on $BaMn_2As_2$ (and $BaMn_2P_2$) that we propose. However, our principal predictions, about diffraction by Dirac multipoles, cannot be derived from the theoretical framework employed by Watanabe and Yanase [13], because it omits all reference to Mn site symmetry. The fatal shortcoming in the framework is compounded by an inadequate account of primary and secondary order parameters.

ACKNOWLEDGMENT

S.W.L. is grateful to Prof. S. P. Collins (Diamond Light Source, Ltd.) for a discussion about the feasibility of the proposed x-ray-diffraction experiments.

APPENDIX

A normalized spherical harmonic $\mathrm{C}^a{}_\alpha(\mathbf{n})$ is defined in the notation adopted by Racah, namely [31,32],

$$\mathrm{C}^a{}_\alpha(\mathbf{n}) = [(4\pi)/(2a+1)]^{1/2}\mathrm{Y}^a{}_\alpha(\mathbf{n}), \tag{A1}$$

where $\mathbf{n}$ is a unit vector, a is the rank, and projections α obey $-a \leqslant \alpha \leqslant a$. The complex conjugate satisfies $[\mathrm{C}^a{}_\alpha(\mathbf{n})]^* = (-1)^\alpha \mathrm{C}^a{}_{-\alpha}(\mathbf{n})$. A similar relation holds for Hermitian multipoles with $\langle \mathrm{O}^K{}_Q\rangle = (-1)^Q\langle \mathrm{O}^K{}_{-Q}\rangle^*$.

A spherical tensor of rank K is constructed from the product of tensors A^a and B^b using

$$\begin{aligned}\{\mathrm{A}^a \otimes \mathrm{B}^b\}^K{}_Q &= \sum_{\alpha,\beta}\mathrm{A}^a_\alpha \mathrm{B}^b_\beta (a\alpha b\beta|KQ)\\ &= (1/2)\sum_{\alpha,\beta}\Big\{\big[\mathrm{A}^a_\alpha \mathrm{B}^b_\beta + \mathrm{B}^b_\beta \mathrm{A}^a_\alpha\big]\\ &\quad + \big[\mathrm{A}^a_\alpha \mathrm{B}^b_\beta - \mathrm{B}^b_\beta \mathrm{A}^a_\alpha\big]\Big\}(a\alpha b\beta|KQ).\end{aligned} \tag{A2}$$

In the second equality the product of tensors is a sum of Hermitian and anti-Hermitian operators. The latter is zero if A^a and B^b commute, but $\{\mathrm{A}^a \otimes \mathrm{B}^b\}^K{}_Q$ is not Hermitian even in this case. The Clebsch-Gordan coefficient in (A2) and Wigner 3-j symbol are purely real quantities related by [31,32]

$$(a\alpha b\beta|KQ) = (-1)^{-a+b-Q}\sqrt{(2K+1)}\begin{pmatrix} a & b & K\\ \alpha & \beta & -Q\end{pmatrix}. \tag{A3}$$

The tensor product of entangled spin and orbital degrees of freedom used in Sec. IV of the main text is $\langle \mathbf{H}^{K'}(K)\rangle \propto \{\mathbf{S}\otimes \mathbf{C}^K(\mathbf{n})\}^{K'}$ with a proportionality factor chosen to make $\mathbf{H}^{K'}(K)$ Hermitian.

A matrix element of a spherical tensor operator obeys the Wigner-Eckart theorem [31,32]. Denoting such an operator by $\mathrm{O}^K{}_Q$,

$$\begin{aligned}\langle JMsl|\mathrm{O}^K{}_Q|J'M's'l'\rangle &= (-1)^{J-M}(Jsl||\mathrm{O}^K||J's'l')\\ &\quad\times\begin{pmatrix} J & K & J'\\ -M & Q & M'\end{pmatrix},\end{aligned} \tag{A4}$$

in which $(Jsl||\mathrm{O}^K||J's'l')$ is a so-called reduced matrix element (RME), and total angular momentum $\mathbf{J} = \mathbf{s} + \boldsymbol{l}$. Note that $(J - M)$ is always an integer. Should O^K be a function of orbital operators alone,

$$\langle lm|\mathrm{O}^K{}_Q|l'm'\rangle = (-1)^{l-m}(l||\mathrm{O}^K||l')\begin{pmatrix} l & K & l'\\ -m & Q & m'\end{pmatrix}. \tag{A5}$$

An RME of an operator with defined discrete symmetries obeys two fundamental identities that apply for both J integer and J half-integer states [33]:

$$(Jsl||\mathrm{O}^K||J's'l') = (-1)^{J'-J}(J's'l'||\mathrm{O}^K||Jsl)^*, \tag{A6a}$$

$$(J's'l'||\mathrm{O}^K||Jsl) = (-1)^{J-J'}\sigma_\theta\sigma_\pi(-1)^K(Jsl||\mathrm{O}^K||J's'l'). \tag{A6b}$$

The first identity holds for a Hermitian operator, while the second identity is independent of the specific operator, because it depends solely on definitions of time-reversed states and parity [17,33]. In (A6b) $\sigma_\theta = \pm 1$ ($\sigma_\pi = \pm 1$) is the time signature (parity signature) of O^K. In most cases of interest, a RME is either purely real or purely imaginary, in which case (A6) tells us that $[\sigma_\theta\sigma_\pi(-1)^K] = \pm 1$, where the upper sign applies to purely real RME and the lower sign applies to a purely imaginary RME of a Hermitian operator.

The RME of a tensor product (A2) formed by spin and spatial variables z^a and y^b, respectively, is usefully written in terms of a unit tensor [17,33]. We define such an RME as

$$(\theta||\{z^a \otimes \mathrm{y}^b\}^K||\theta') = (\mathrm{s}||z^a||s)(l||y^b||l')\mathrm{W}^{(a,b)K}(\theta,\theta'), \tag{A7}$$

where $\mathrm{W}^{(a,b)K}(\theta,\theta')$ is the unit tensor and composite labels $\theta = Jsl$ and $\theta' = J's'l'$. A tensor product is generally not a Hermitian operator, even when both parent operators, z^a and y^b, are Hermitian. A Hermitian operator can be constructed from a tensor product, however, with a little ingenuity. Introduction of a complex phase factor suffices for commuting operators. In the particular case of one electron [33],

$$\begin{aligned}\mathrm{W}^{(a,b)K}(\theta,\theta') &= [(2j+1)(2K+1)(2j'+1)]^{1/2}\\ &\quad\times\begin{Bmatrix} s & s & a\\ l & l' & b\\ j & j' & K\end{Bmatrix},\end{aligned} \tag{A8}$$

in which $s = 1/2$ yields $a = 0$ or 1, with $(s||z^0||s) = \sqrt{2}$ or $(s||z^1||s) = \sqrt{(3/2)}$ in (A7). The magnitude of the $9j$ symbol in (A8) is unchanged by an even or odd exchange of columns or rows, while its sign is changed by a factor $(-1)^{\Re}$ with an odd exchange of columns or rows where $\mathrm{Re} = (1 + a + l + l' + b + j + j' + K)$ [31]. A single operator in a coupled scheme, using spin and orbital quantum labels, possesses a RME proportional to a $6j$ symbol [31]. We use S-L coupling, for which the RME of an operator O^K working only on part 2 (orbital variables) is

$$(J'sl'||\mathrm{O}^K||Jsl) = (-1)^{s+l+J'+K}[(2J+1)(2J'+1)]^{1/2} \times (l'||\mathrm{O}^K||l)\begin{Bmatrix} l' & J' & s \\ J & l & K \end{Bmatrix}. \quad \text{(A9)}$$

The result (A9) provides $(J'sl'||\{\mathbf{L}\otimes\mathbf{n}\}^K||Jsl)$ in terms of $(l'||\{\mathbf{L}\otimes\mathbf{n}\}^K||l)$, which can be obtained by straightforward use of (A5) for the tensor product derived from (A2).

[1] S. L. Brock, J. E. Greedan, and S. M. Kauzlarich, J. Solid State Chem. **113**, 303 (1994).
[2] Y. Singh, A. Ellern, and D. C. Johnston, Phys. Rev. B **79**, 094519 (2009).
[3] D. N. Astrov, Zh. Eksp. Teor. Fiz. **38**, 984 (1960) [Sov. Phys. JETP **11**, 708 (1960)].
[4] I. Dzyaloshinskii, Zh. Exp. Teor. Fiz. **37**, 881 (1959) [Sov. Phys. JETP **10**, 628 (1959)].
[5] R. R. Birss, *Symmetry and Magnetism* (North-Holland, Amsterdam, 1966).
[6] A. P. Cracknell, *Magnetism in Crystalline Materials* (Pergamon, Oxford, 1975).
[7] M. Fiebig, J. Phys. D **38**, R123 (2005).
[8] S. Di Matteo, Y. Joly, A. Bombardi, L. Paolasini, F. de Bergevin, and C. R. Natoli, Phys. Rev. Lett. **91**, 257402 (2003).
[9] D. D Khalyavin, S. W. Lovesey, P. Manuel, F. Krüger, S. Rosenkranz, J. M. Allred, O. Chmaissem, and R. Osborn, Phys. Rev. B **90**, 174511 (2014).
[10] K. A. Milton, Rep. Prog. Phys. **69**, 1637 (2006).
[11] S. V Gallego *et al.*, J. Appl. Cryst. **45**, 1236 (2012).
[12] J. Hubbard and W. Marshall, Proc. Phys. Soc. **86**, 561 (1965).
[13] H. Watanabe and Y. Yanase, Phys. Rev. B **96**, 064432 (2017).
[14] A. H. Morrish, *Canted Antiferromagnetism: Hematite* (World Scientific, Singapore, 1994).
[15] S. W. Lovesey and D. D. Khalyavin, J. Phys.: Condens. Matter **27**, 495601 (2015).
[16] P. J. Brown, in *International Tables for Crystallography*, edited by E. Prince (Springer, New York, 2004), Vol. C, pp. 454–461.
[17] S. W. Lovesey, E. Balcar, K. S. Knight, and J. Fernández Rodríguez, Phys. Rep. **411**, 233 (2005).
[18] S. W. Lovesey, Phys. Scr. **90**, 108011 (2015).
[19] S. W. Lovesey and D. D. Khalyavin, J. Phys.: Condens. Matter **29**, 215603 (2017).
[20] Y. Joly, Phys. Rev. B **63**, 125120 (2001).
[21] Jun-ishi Igarashi and T. Nagao, Phys. Rev. B **80**, 054418 (2009).
[22] M. Fechner, M. J. A. Fierz, F. Thöle, U. Staub, and N. A. Spaldin, Phys. Rev. B **93**, 174419 (2016).
[23] J. An, A. S. Sefat, D. J. Singh, and M.-H. Du, Phys. Rev. B **79**, 075120 (2009).
[24] C. Zheng and R. Hoffmann, J. Solid State Chem. **72**, 58 (1988).
[25] J. Fernández-Rodríguez, V. Scagnoli, C. Mazzoli, F. Fabrizi, S. W. Lovesey, J. A. Blanco, D. S. Sivia, K. S. Knight, F. de Bergevin, and L. Paolasini, Phys. Rev. B **81**, 085107 (2010).
[26] V. Scagnoli *et al.*, Science **332**, 696 (2011).
[27] U. Staub, C. Piamonteze, M. Garganourakis, S. P. Collins, S. M. Koohpayeh, D. Fort, and S. W. Lovesey, Phys. Rev. B **85**, 144421 (2012).
[28] B. J Kim *et al.*, Science **323**, 1329 (2009).
[29] L. C. Chapon and S. W. Lovesey, J. Phys.: Condens. Matter **23**, 252201 (2011).
[30] P. Bourges, Y. Sidis, and L. Mangin-Thro, Phys. Rev. B **98**, 016501 (2018).
[31] D. A. Varshalovich, A. N. Moskalev, and V. K. Khersonskii, *Quantum Theory of Angular Momentum* (World Scientific, Singapore, 1988); A. R. Edmonds, *Angular Momentum in Quantum Mechanics* (Princeton University, Princeton, NJ, 1960).
[32] I. V. Hertel and C.-.P Schulz, *Atoms, Molecules and Optical Physics* (Springer-Verlag, Heidelberg, 2015), Vol. 1.
[33] E. Balcar and S. W. Lovesey, *Introduction to the Graphical Theory of Angular Momentum*, Springer Tracts in Modern Physics Vol. 234 (Springer, New York, 2009).